JCTC Journal of Chemical Theory and Computation

ARTICLE

pubs.acs.org/JCTC

On the Origin of the Chiro-Optical Activity in Supramolecular Assemblies: A Quantum Chemical Study of C_3 Octopolar Systems

Belén Nieto-Ortega,[†] Juan Casado,[†] Juan T. López Navarrete,[†] Gunter Hennrich,[‡] and Francisco J. Ramírez*[,†]

[†]Departamento de Química Física, Universidad de Málaga, 29071-Málaga, Spain

[‡]Departamento de Química Orgánica, Universidad Autónoma de Madrid, Cantoblanco, 28049-Madrid, Spain

Supporting Information

ABSTRACT: First-principles quantum chemical approach has been used to understand the origin of the chiro-optical signal induced by the chiral aggregation of an achiral chromophore. The study was focused in predicting the circular dichroism (CD) spectra of different π-stacked columnar oligomers built with C_3 star-shape molecular bricks. We studied the influence of the relevant structural self-assembly parameters on the CD spectra (i.e., the number of units, the rotation angle and the intermonomer distance). A detailed analysis was based on the MO topologies and the magnetic and electric transition dipole moments, the vectors which determine the CD intensities, has been conducted. We have rationalized the influence of the various structural factors of supramolecular self-assemblies in connection with the nature of their CD spectroscopic signal, which provides new avenues for structure−spectroscopic relationships.

1. INTRODUCTION

Chiral molecular materials have become a major point of interest for scientists.[1−4] Many of them are formed by organic molecules assembled into highly ordered helical superstructures in which they stack one above the other forming columns.[5−7] This conformation gives interesting properties to the material, as the charge transportation along the column axis, useful in organic-based electronic devices.[8,9] The presence of a stereogenic center in these molecules leads to the preferential formation of one of the two possible helices (enantiomeric excess) and to a noticeable enhancement of the ability to absorb left/right circularly polarized light differently;[10−12] it is to say, the material is endowed with chiro-optical properties. The manipulation of these properties associated with the particular solid state structure provides a new avenue for applications.[13−15] It turns out that the study of the supramolecular chirality is an essential step to develop new materials and future applications in diverse fields or organic electronics.

The chiro-optical spectroscopy (COS) has become a very useful tool to explore the structure of supramolecular assemblies, such as proteins, nucleic acids, or liquid crystals.[16−20] As a first glance, the origin of the supramolecular chiro-optical signal is explained by the excitonic coupling theory between interacting chromophores.[10] However, aspects as the growing of these three-dimensional (3D) structures and how COSs monitorize this process or the sensitivity of the chiro-optical signal with respect to the structural markets of the assemblies have not been thoroughly addressed up to now. Thus, while many molecular mechanics studies are routinely conducted to predict the helical behavior of chiral aggregates, first-principles quantum chemical studies addressing the same phenomena in aggregates are scarce to our knowledge. In this work we performed a detailed analysis of the electronic circular dichroism (CD) spectra, as predicted by quantum chemistry calculations, of several helical superstructures. As the molecular brick we have chosen a C_3 octopolar molecule constituted by a central benzene ring substituted by three aryl-acetylene groups in alternating positions forming a star-shaped 2D configuration, Figure 1. A subtle structural difference in one of the three tails was included in order to control the rotation angle. Thus, two tails were phenyl-acetylene groups, while the third was a pyridine-acetylene one (Figure 1).

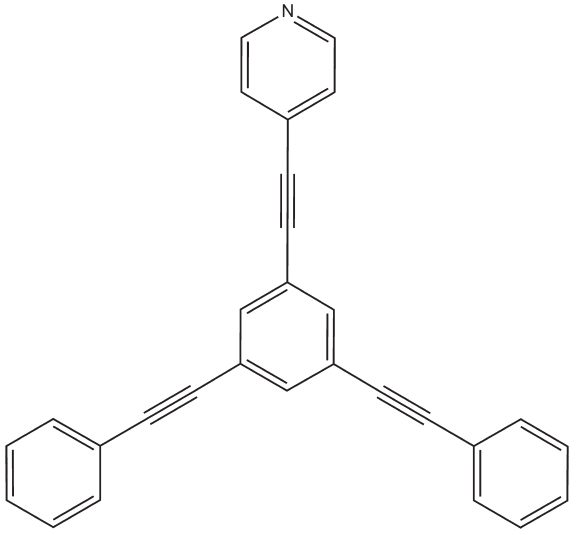

Figure 1. Molecular structure of the C_3 star-shaped octopolar molecular studied in this work.

These C_3 aromatic planar structures can be easily functionalized by attaching aliphatic side chains containing asymmetric

Received: July 22, 2011
Published: September 02, 2011

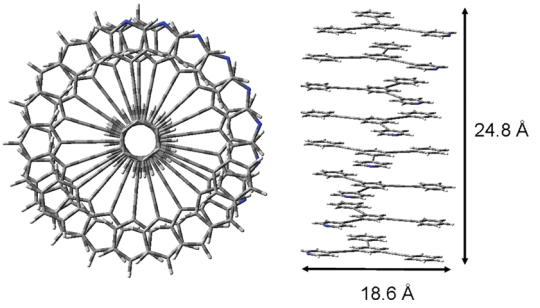

Figure 2. Front and side views of the columnar π-stacked octamer.

carbon atoms, which can act as stereogenic centers to promote chiral superstructures. From an experimental point of view, the stereocenters are effectively required to provide chiral activity to the material. They are not essential, nevertheless, in a theoretical study, as we can easily model any chiral superstructure from an achiral molecule as that displayed in the Figure 2. Nonetheless, the absence of intrinsic chirality in the molecules provides a significant advantage: The recorded chiral display will be fully induced by the assembly. It is then feasible and even advisible to provide results, at a theoretical level, about chiral assemblies of nonchiral molecules; this in turn will reduce the computational costs, thus allowing us to study more complex systems.

A variety of methods and strategies can be used to build a superstructure based on a C_3 star-shape molecule. Studies on these materials have been recently performed in our laboratory,[21] providing experimental evidence that the main stabilizing force in C_3-based supramolecular structure is the face-to-face π-stacking between the aromatic groups, which are spectroscopically well-defined achiral chromophores whose structures are often slightly perturbed when aliphatic side chains are attached. Following the previous report of Meijer et al.,[22,23] we have focused our study on a right-handed helical columnar structure with a rotation angle of 20°. As shown in Figure 2 for one of the studied oligomers, these discotic structures allow for establishing strong π-stacking attractions and highly packed structures that can exhibit noticeable increases of their chiral features. The distance between monomers was established at 3.5 Å, which is an intermediate value of the estimated optimal range for π-stacking interactions (3.3−3.7 Å).[24] The π-stacking strength was settled from a basic stabilization energy calculated from the following equation:

$$E_{sta} = \frac{E_{olig}}{n} - E_{mon}$$
$$(n = \text{number of monomers in the oligomer})$$

The E_{sta} values, which have been included as Table TS1 of Supporting Information, increase with the oligomer size. We have then built a series of stable columnar oligomers, up to the octamer, able to generate nanometer fibers with a mean diameter of 18.6 Å. The origin of the chiro-optical signal in these supramolecular systems was analyzed by predicting their CD spectra using DFT calculations in combination with ab initio methodology.

2. COMPUTATIONAL METHODS

The Gaussian'09 package of programs[25] was used for DFT quantum chemical calculations. The Becke's three parameter (B3)[26] gradient-corrected exchange functional was used, and the nonlocal correlation was provided by the Lee−Yang−Parr (LYP) expressions.[27,28] To give account of charge-transfer excitations, we used the Coulomb-attenuating hybrid method (CAM-B3LYP),[29] which includes the Hartree−Fock and the Becke exchanges as a variable ratio depending on the intermolecular distance. It has been demonstrated that this method gives an improved description of long-range interactions.[30−35] Structural optimizations and spectroscopic features were calculated using the split-valence 3-21 g(d) basis set.[36,37] At this level of calculation, data up to the octamer were available, while the essence of the chiro-optical signal was preserved. This was checked by comparing CD spectra for a right-handed trimer, with a rotation angle of 20°, at different ab initio methodologies, as 6-31 g(d,p) or cc-pvdz. These spectra are included as Figure FS1 of Supporting Information.

The minimum-energy structure of the monomer was achieved by allowing all the geometrical parameters to vary independently. Optimization gave us a fully planar star-shape structure in which the central benzene and the C≡C bonds are insensible to the slight structural modification introduced in one of the three tails (the pyridine group), being all the benzene C−C and the C≡C distances of 1.398 and 1.205 Å, respectively. Electronic excitation energies of the different oligomers were obtained by using the time-dependent DFT (TDDFT) formalism[38,39] for which up to the 50 low-lying energy states were considered. The origin of the electronic chiral activity was explained at the light of the excitonic structure and the topology of the involved molecular orbitals (MO).

3. RESULTS AND DISCUSSION

The electronic absorption and CD spectra of the π-stacked columnar oligomers studied with rotation angle of 20° are shown in Figure 3. The intensity of all the spectra was divided by the number of monomers to remove the effect of the oligomer size. A first result is highlighted when comparing the panels of Figure 3: The two spectral series show opposite trends with respect to the oligomer size. Thus, while the intensity of the nonchiral signal decreases when increasing the number of oligomers, the chiral signal is clearly enhanced. The number of active bands also shows a different trend. The absorption spectra seem to show a single active band throughout the series whose wavelength monotonically decreases from the monomer to the octamer. However, no less than seven bands have appreciable CD intensities for the dimer, which are gradually removed when more C_3 units are stacked until showing only a bisignate, or Cotton band, near the wavelength of the absorption maximum of the octamer.

Figure 4 (left panel) shows the wavelength dispersion with respect to the number of monomers. The resulting trend suggests that an asymptote is almost reached for the octamer, from which we can deduce a blue-shift limit not greater than 10 nm in the case of an ideal infinite helix. The intensity changes with respect to the oligomer size, measured either on the absorption maxima or on the positive CD signals, are plotted in Figure 4 (right panel). This graphic contains a second and remarkable difference between the chiral and nonchiral spectra: Aside from the slope signs, only the absorption intensities show saturation when increasing the number of monomers, while the intensity of the CD signal shows a quasi-lineal behavior, and no saturation is anticipated. Thus, these results highlight the sensitivity of the CD spectra to long-range interactions,[40−42] as it gives account of the self-assembly even when the nonchiral signal is no longer able to.

If we defined the exciton bandwidth (W) as the energy difference between the bisignate maximum and minimum,[43] a relationship between W and the number of units of the helical

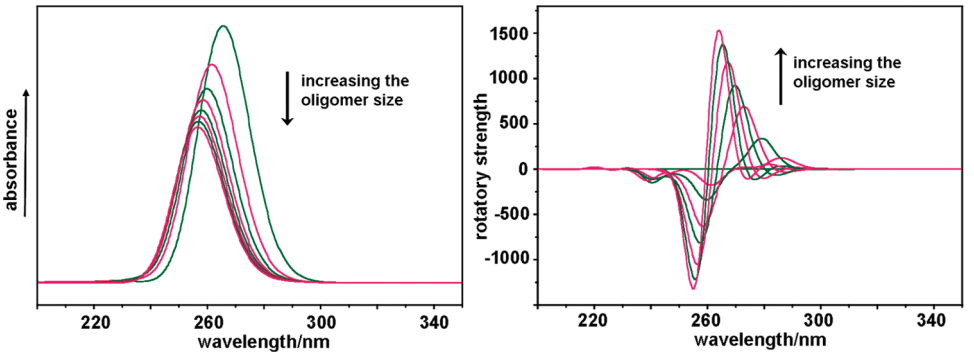

Figure 3. Electronic absorption (left panel) and CD (right panel) spectra of the π-stacked columnar oligomers, from one to eight monomers, with a rotation angle between stacked monomers of 20°. All the spectra were normalized to the number of monomers. Alternant colors are used to follow the spectral trend.

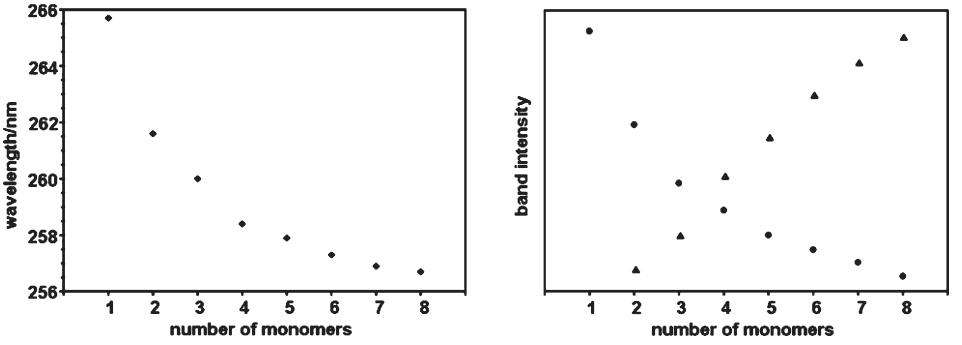

Figure 4. Left panel: graphic of the wavelength (at the absorption maxima) as a function of the number of monomers. Right panel: graphic of the intensity of the absorption band (circles) and the CD positive feature (triangles) as a function of the number of monomers.

Table 1. Exciton Bandwidth (W) Measured for the Main CD Bisignate of Each Oligomer

	W (meV)
dimer	430
trimer	340
tetramer	230
pentamer	220
hexamer	180
heptamer	150
octamer	110

assembly can be easily achieved. The calculated values for this series, Table 1, monotonically decrease when increasing the number of stacked units, thus demonstrating that W is useful in evaluating the interaction between the monomers.

The parameter W is also modulated by the distance between monomers (D). Accordingly with the following equation[18] which relates D with the rotational strength (R):

$$R(\pm) = \pm \frac{\varepsilon \mu^2 D}{4\hbar} \sin\alpha \sin\gamma \sin\tau$$

D is greater when R is increased. In this equation, τ is the rotation angle between monomers (here +20°), while α and γ are the angles between the major helix axis and the electric transition dipole moments (ETDM) of two adjacent monomers. As will be discussed below, the ETDM vectors of the main transitions are almost perpendicular to the helix axis, so that α and γ are near 1 (namely, α = 83.8° and γ = 82.5° for the positive feature at 279 nm). This means that, in the oligomers studied, the rotational strength is largely dependent on the rotation angle τ.

The last result, nevertheless, would lead to the paradox that at $D = \infty$, the CD signal would have an infinite intensity. To compensate this effect, we have to consider the effect of D on the exciton bandwidth. This is given by the equation:[18]

$$W = \varepsilon \pm \frac{\mu^2(\sin\alpha \sin\gamma \cos\tau + 2\cos\alpha \cos\gamma)}{D^3} \approx \varepsilon \pm \frac{\mu^2 \cos\tau}{D^3}$$

where ε is the wavelength of the electronic transition in the monomer. As the fraction goes to 0 when $D \rightarrow \infty$, cancellation between the positive and the negative features of the bisignate will occur when increasing the intermonomer distance, and the Cotton effect disappears. We studied this phenomenon by calculating the CD spectra of the trimer at different D values, from 3 to 8 Å, which are shown in Figure 5. From the spectrum at 3 Å, a progressive increasing of the CD signal (R) together with a reduction of the exciton bandwidth (W) is predicted when increasing D up to 5 Å. However, and accordingly with the aforementioned equations, while W continues to decrease at 8 Å, the CD intensity is noticeably reduced as a consequence of the exciton cancellation. We have then obtained useful spectroscopic−structural relationships, as both the intensity of the CD signal and the width of the Cotton effect can be related, even at a quantitative level, with the intermonomer packing.

The results discussed above can be qualitatively interpreted from a molecular orbital analysis. We focus on the trimer as a simple stacked model. As can be seen in Figure 6 (left panels), the aforementioned bisignate is the envelope of four electronic transitions with excitation energies of 279.1 (D1) and 278.6 nm (D2) for the positive feature and 260.6 (D3) and 259.0 nm (D4) for the negative one. Among them, only D3 and D4 have nonvanished oscillator strength values, being the origin of the main absorption band in the UV−vis spectrum (Figure 6). These four excitations are described by the contribution of several monoelectronic transitions which involve up to 18 molecular orbitals, from MO289 to MO306, with MO297 being the highest occupied molecular orbital (HOMO). A complete summary of quantitative assignments for D1−D4 and topologies of the 289−306 MO are included as Table TS2 and Figure FS2, respectively, in Supporting Information. Figure 6 (right panels) also shows the calculated spectra for the trimer with a rotation angle of −20°, forming a left-handed helix. Its CD spectrum is a mirror image of the calculated one for the right-handed helix, while the absorption spectra are identical, which confirms that the chiro-optical signal is only due to the supramolecular assembly.

The similar optical activity of the two bisignate branches together with their extremely different absorption intensities allows us to anticipate that the positive CD feature should be the result of two magnetic dipole allowed (mda) transitions (D1 and D2) while the negative band would be due to two electric dipole allowed (eda) ones. This conclusion is, therefore, depending of the angle θ between the corresponding magnetic and electric transition dipole moments (MTDM and ETDM, respectively), which determine the final CD activity of any electronic transition $\varphi_i \rightarrow \varphi_j$ by means of the Rosenfeld equation:[18]

$$\int \Delta\varepsilon dv \propto R_{ij} \approx \vec{\mu_{ij}} \cdot \vec{m}_{ji} = |\vec{\mu_{ij}}| \cdot |\vec{m}_{ji}| \cdot \cos\theta$$

where R_{ij} is the rotational strength (which is related with the intensity of the chiro-optical signal), μ is the EDTM for the $\varphi_i \rightarrow \varphi_j$ transition, m is the MDTM for the reverse transition, and θ is the angle between these two magnetic dipole moments. As can be seen in the equation, the R_{ij} value will be positive if θ is smaller than 90°, negative if larger, and null if the vectors are perpendicular. In an achiral monomer, either $m = 0$, $\mu = 0$, or $\theta = 90°$, so all its electronic transitions are CD silent, as successfully predicted in our case. However, a chiral assembly will modify these parameters, and as a consequence, an induced CD signal will appear.

Thus, to find out the true origin of the chiro-optical activity in the trimer (and by extension in the rest of oligomers), we need to calculate the EDTM and the MDTM vectors. They are drawn in Figure 7 for the D1−D4 electronic transitions. The components of each vector can be found in Table TS3 of Supporting Information. First we pay attention to D1 and D2 transitions. As represented in Figure 7, their calculated EDTM and MDTM vectors are within the *xy* molecular plane, being the θ values 2.4 and 4.2°, respectively. Hence the R_{ij} is positive. The modulus of their MDTMs is significantly greater than for their EDTMs, and as a consequence, we can conclude that D1 and D2 are markedly mda transitions with weak contributions from the EDTM.

The calculated MTDM and EDTM of D3 and D4 transition are also within the *xy* plane; however, their angles are rather different, 146.0 and 167.4°, respectively. The cosines of these angles are similar, in absolute values, to those of D1 and D2, but now the signs, and consequently the R_{ij} values, are negative. The MDTM modulus is here much lower than the EDTM one, what means that not only the sign of the band, but the origin of the CD signal is inverted. D3 and D4 are then eda transitions, that is to say, the nature of their chiro-optical activity is largely electric, having a weak contribution of the magnetic component. This is also the cause of their strong absorption intensities, which successfully explains the spectra of Figure 6.

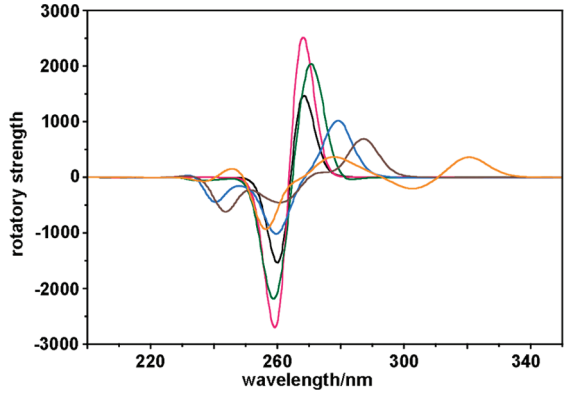

Figure 5. Calculated CD spectra of the right-handed (20° rotation angle) trimer at different intermomomer distances (D): 3.0 (orange), 3.3 (brown), 3.5 (blue), 4.0 (green), 5.0 (red), and 8.0 Å (black).

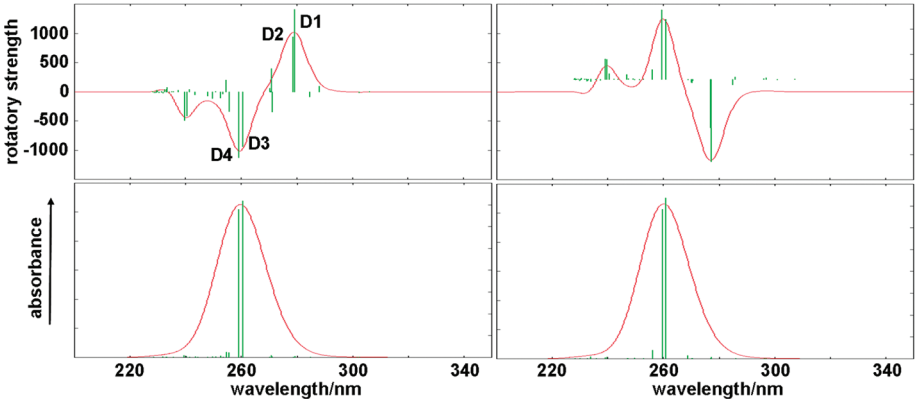

Figure 6. Bar representation of the exciton energies of the transitions calculated for the trimer with a rotation angle between stacked monomers of 20° (left panels) and −20° (right panels). The height of the green bars is proportional to the rotational strength.

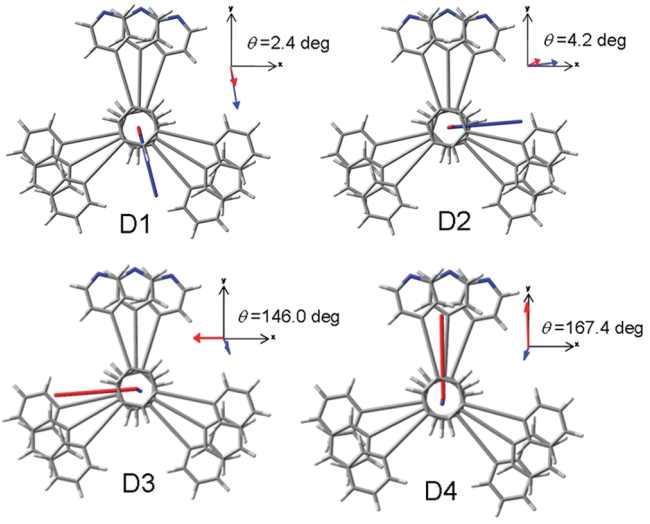

Figure 7. EDTM (red vectors) and MDTM (blue vectors) associated to D1−D4 electronic transitions of the trimer.

Table 2. Calculated Modulus of EDTM and MDTM Vectors Associated to the D1−D4 Monoelectron Transitions[a]

	EDTM				MDTM			
	D1	D2	D3	D4	D1	D2	D3	D4
dimer	1.26	0.81	24.43	23.78	12.7	13.4	0.63	0.77
trimer	1.63	1.01	18.49	17.93	16.3	17.5	1.13	1.21
tetramer	2.09	1.17	12.65	12.93	19.3	21.3	1.64	1.46
pentamer	2.16	0.95	10.23	10.10	20.0	18.7	1.40	2.25
hexamer	2.27	0.97	9.77	9.20	21.4	21.8	1.52	2.22
heptamer	2.27	0.88	8.07	7.44	21.8	23.4	1.85	2.22
octamer	2.18	0.78	6.24	5.48	21.2	24.4	2.96	4.37

[a] All values have been divided by the number of monomers in each case.

The MDTM and EDTM moduli of the electronic transitions D1−D4 allow us to explain the spectral intensities shown in Figure 3. Table 2 summarizes the values for the series of oligomers studied, all of them normalized to the number of monomers as performed for the calculated spectra. Accordingly with the behavior of the Cotton effect, the MDTM modulus grows up when increasing the oligomer size, showing similar values for the four transitions. On the contrary, the EDTM modulus is noticeably higher for D3 and D4 than for D1 and D2 doublets and, in agreement with the absorption spectra, the values for D3 and D4 go down with the number of monomers. Since EDTMs for D1 and D2 do not show a clear trend within the series, and taking into account that the θ values do not appreciably vary with respect to those shown in Figure 3 for the trimer, we can conclude that the increasing of the CD signal is largely caused by the enhancement of the magnetic coupling between the stacked monomers.

A further explanation of the different nature found for the two components of the Cotton effect in these oligomers can be reached by analyzing the MO of the trimer involved in the D1−D4 transitions. In an eda mechanism, only the displacement of electric charge during the excitation is relevant, while a mda transition is characterized by the magnitude of the magnetic moment. This means that in a mda transition, we must focus our attention on the electric charge rotation perpendicular to the molecular planes, which can be evaluated in light of the MO topologies associated to the monoelectronic transitions and their relative weights (Figure FS2 and Table TS2, respectively, of Supporting Information). The analysis can be summarized in the following points:

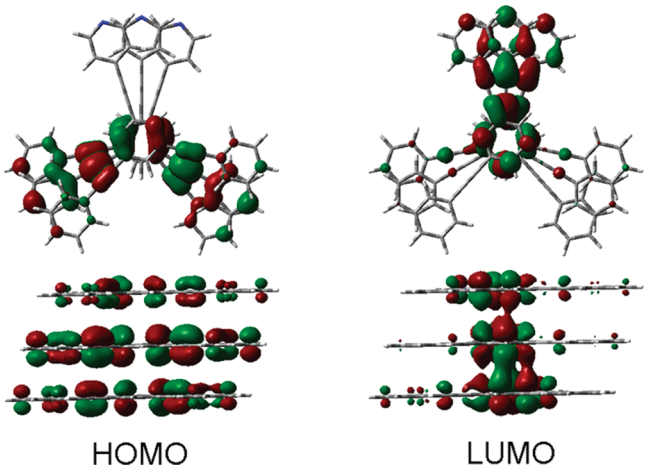

Figure 8. Frontal and side views of the HOMO and LUMO topologies calculated for the trimer.

(i) All MO analyzed belong to the π-bond system. In the basis of the electron density distribution, they can be classified into two groups. The 289, 291, 293, 298(LUMO), and 299 MOs have stacking topologies because the interplane electronic density is reinforced. The rest of MOs exhibit nodal planes in the intermonomer regions, so they are antistacking topologies. This fact can be observed for HOMO and LUMO, as representative examples, in Figure 8.

(ii) The monoelectron transitions can connect two similar MO or not. Only in the last case we have charge rotation and, consequently, magnetic moment. This can be supported by calculating the total contribution of transitions with charge rotation in the two mda transitions, D1 and D2, being 23 and 35%, respectively, while these values are much lower in the two eda transitions, namely 3 and 7% for D3 and D4, respectively. These values also show the same trend as the calculated MDTM (see Table TS3, Supporting Information).

(iii) As can be observed in Figure 8, and more extensively in Figure FS2, Supporting Information, in all the monoelectron transitions, the electronic density flows away from the C≡C bonds. Electronic excitations are then associated to structural changes in which the C≡C bonds become longer while the adjacent C−C ones shorten, and as a consequence, the molecular structure in the excited state is expected to be more rigid than in the ground state. We expect this effect affects to the benzene rings, which undergo an aromatic-to-quinoid transition.

The last hypothesis has been investigated by comparing the optimized structures of the monomer in the ground state and in the first excited state, Table 3. They were calculated using the restricted configuration interaction (singlet) approach (RCIS) in combination with the 3-21 g(d) basis set. The quinoid structure is only observed for one of the three aryl-acetylene moiety and the central benzene ring, remaining the bond lengths of the other

Table 3. Relevant Bond Lengths (in Å) Calculated for the Ground State and the First Excited State of the Monomer

bond	S_0	S_1
$C_7{\equiv}C_8$	1.192	1.246
C_4-C_7	1.432	1.371
C_8-C_9	1.431	1.371
$C_2{=}C_3$	1.382	1.369
$C_3{=}C_4$	1.392	1.430
$C_{10}{=}C_{11}$	1.389	1.376
$C_9{=}C_{10}$	1.389	1.427

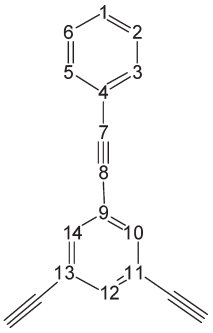

two tails unchanged. This is in agreement with the topology of most of the MO, in which the electronic density is concentrated over one of the aryl-acetilene groups. As predicted, the central ring distorts its hexagonal symmetry in the S_1 state, thus presenting a quinoid structure with respect to the involved aryl-acetylene group. Within this branch, the C≡C bond is lengthened, while the two adjacent C−C bonds are similarly shortened. This in turn modifies the outer benzene ring, which presented some quinoidization in the ground state, also in the aromatic-to-quinoid sense.

In the precedent paragraphs, we have shown that the CD signal produced by a 20° right-handed helices was largely due to either a magnetic or an electric mechanism. Looking for a relationship between the torsion angle of the chromophores and the chiro-optical response, we have studied a similar series of π-stacked columnar oligomers with a rotation angle between monomers of 120° and maintaining the intermonomer separation of 3.5 Å. Since this angle matches the pseudosymmetry angle of the C_3 molecules, the only structural element to characterize the helices is now the position of the pyridinium ring, without which no rotation angle could be defined, and in consequence, we would have no helix. In order to check the ability of the calculation method in this new scenario, we have first calculated the CD spectrum of a 120° right-handed tetramer in which the pyridine ring was replaced by a benzene one, that is to say, a columnar structure in which no rotation between monomers can be appreciated. Figure 9 compares the CD spectra of both tetramers, with or without pyridine. As can be seen, the chiral response in the last case is negligible, which demonstrates that our methodology is able to detect a helical symmetry even though it depends on a subtle atomic substitution in a moderate-size chromophore.

Figure 10 displays the normalized electronic absorption and CD spectra calculated for the new series. Comparing with the spectra of Figure 3, noticeable deviations are observed. While the UV−vis spectra of helices with 2−5 units are quite similar for both rotational angles, those with 6−8 units show a dramatic intensity reduction. The analysis of the CD spectra is more troublesome, as they do not exhibit a fair trend. A Cotton effect with a positive band at 259 nm and a negative one about 250 nm is the dominant feature in tetramer and pentamer, whose spectra also show very similar intensities after normalization. The pentamer shows a second, less intense, negative band at 271 nm, which undergoes intensity enhancement and blue-shift with the addition of monomers, being the only dominant band, at 266 nm, in the octamer. In a precedent paragraph, exciton cancellation has been related with the increasing of the intermonomer distance.

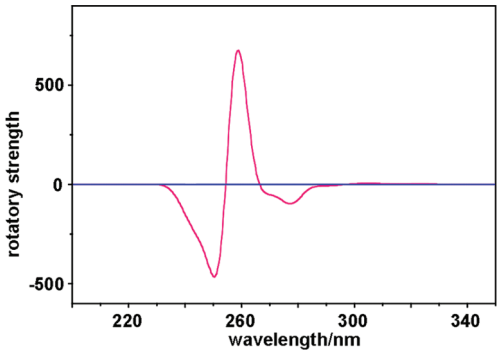

Figure 9. Calculated CD spectra of a π-stacked tetramer whose monomers contain either pyridine (red) or benzene (blue) moieties in one of their branches.

Now we show a similar phenomenon associated with the rotation angle between adjacent monomers, which is highlighted from a critical number of units in the helix.

The electronic transitions involved in the UV−vis and CD spectra of the tetramer (the smaller oligomer showing a clear Cotton effect) are analyzed in Figure 11, which also shows the associated MDTM and ECTM vectors of the most intense transitions. We name D1 and D2 to the positive and the negative strongest transitions, respectively. Figure 11 shows that the difference between the MDTM and EDTM moduli is less pronounced than in the case of the oligomers with rotation angle of 20° (see Figure 7), which indicates that no clear separation between magnetic and electric dipole mechanism exists. In consequence, chiro-optical activity is only predicted for the intense UV−vis absorption, while the positive CD features of the 20° oligomers, which were largely induced by the magnetic mechanism, do not have significant activity in this series. The topology and contribution of the MO associated to the D1 and D2 transitions (included as Figure FS3 and Table TS4 of the Supporting Information, respectively), indicate that in the more relevant monoelectron transitions, the π orbitals change their orientation from the *xy* plane to the *z* axis in both cases. This movement creates a charge rotation within the *xy* plane which explains both transitions are mda, besides being eda as supported by their strong absorption bands.

As the final part, we have applied all the arguments developed in this work to reach a suitable approach to the experimental CD spectrum of a C_3 star-shaped as a representative example of π-stacked columnar superstructures with chiral properties. As aforementioned, the presence of a stereogenic center is now mandatory to give chirality to the aggregates, so that we have selected the molecule shown in Figure 12, named as **PA3Bz**. It is formed by the basic aromatic skeleton studied in this work to which three identical aliphatic side chains, each of them containing an asymmetric carbon atom, were attached to the central benzene ring, with the outer pyridine moiety being replaced by a benzene ring.

In a previous work we reported the synthesis and a spectroscopic study of **PA3Bz**, supported by DFT theoretical calculations on a π-stacked dimer as a basic model of a left-handed helix.[21] The experimental CD spectrum of a solid sample was largely composed by two broad features, namely a positive band at 271 nm and a negative one at 324 nm. In this spectral region we can take on that the CD signal is induced by the formation of chiral superstructures in solid state. By applying the results obtained in

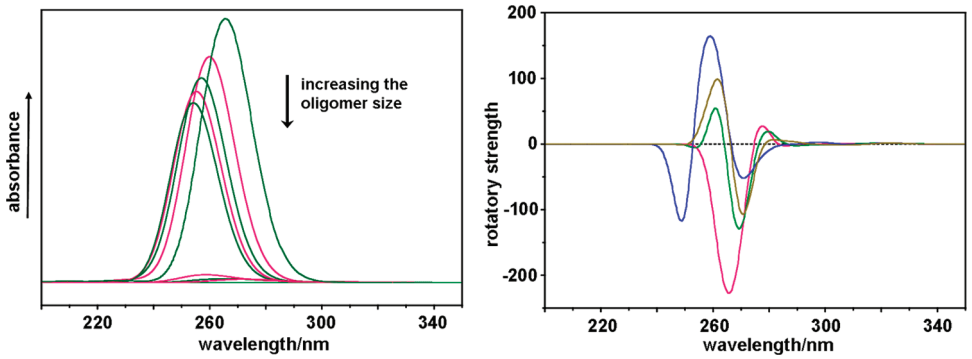

Figure 10. Left: Electronic absorption spectra of the π-stacked columnar oligomers, from 1 to 8 monomers, with a rotation angle between stacked monomers of 120°. Right: CD spectra of the oligomers with 5 (blue), 6 (brown), 7 (green), and 8 (red) monomers. All the spectra were normalized to the number of monomers.

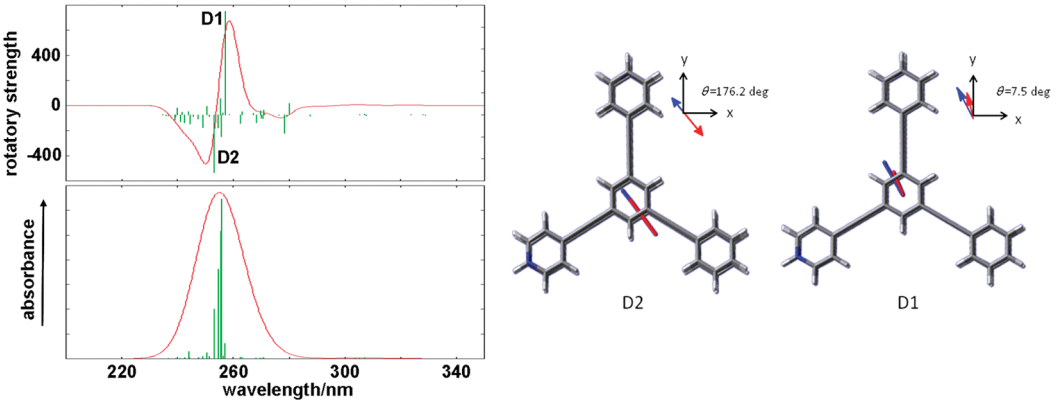

Figure 11. Left: bar representation of the exciton energies of the transitions calculated for a 120° right-handed tetramer. Right: EDTM (red) and MDTM (blue) vectors associated to the most intense electronic transitions.

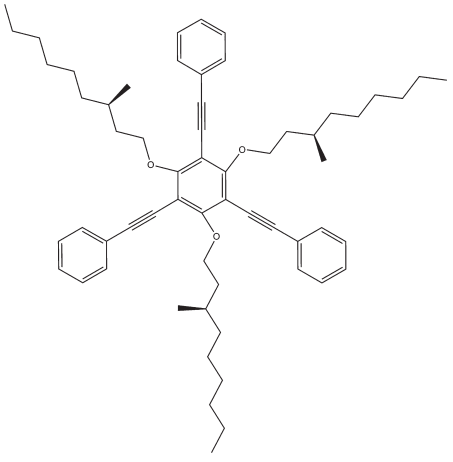

Figure 12. Chemical structure of the molecule **PA3Bz**.

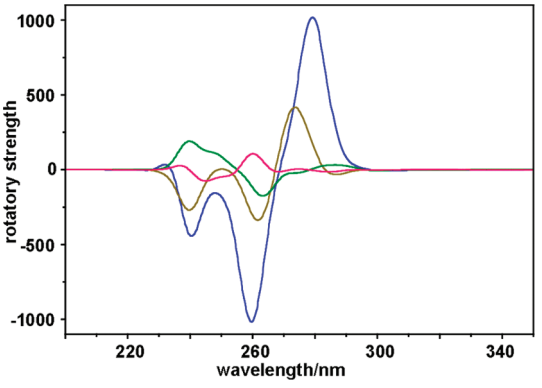

Figure 13. CD spectra of the right-handed trimer with rotation angles between monomers of 20° (blue), 40° (brown), 70° (green) and 120° (red).

this work for columnar helices, this experimental CD spectrum is compatible with a left-handed helix with a separation between stacked monomers of about 3.3−3.2 Å. In order to approach the rotation angle, we investigate the influence of this parameter on the chiro-optical signal. Figure 13 shows the CD spectra of a series of right-handed trimers with different rotation angles from 20 to 120° and using the standard separation between monomers of 3.5 Å. These spectra suggest that more intense Cotton effects are associated with small angles, being negligible the effect over the transition energies. We then chose a rotation angle of 20° to try to reproduce the experimental CD spectrum of **PA3Bz**.

Figure 14 shows a comparison between the experimental CD spectrum of **PA3Bz** from a solid sample and the calculated

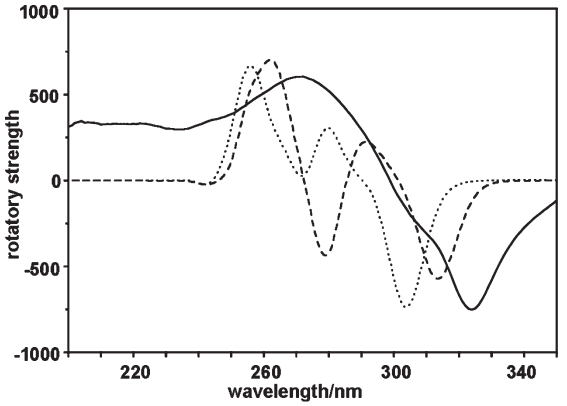

Figure 14. Comparison between the experimental CD spectrum of **PA3Bz** and calculated spectra using CAM-B3LYP/cc-pvdz at different intermonomer distances: 3.3 Å (dotted line) and 3.2 Å (broken line).

spectrum for the model trimer described in the previous paragraph, using the CAM-B3LYP functional in combination with the cc-pvdz ab initio basis set. The striking resemblance existing between these two spectra allows us to suggest that the model helix would be a reliable model of interaction in the solid state, at or at least partially, of the **PA3Bz** molecules.

4. CONCLUSIONS

We have applied a first-principles quantum chemical approach to understand the origin of the chiro-optical signal induced by the chiral aggregation of an achiral chromophore. The study was focused in predicting the CD spectra of different π-stacked columnar oligomers built with C_3 star-shape molecular bricks. We studied the influence of the relevant structural self-assembly parameters on the CD spectra (i.e., the number of units, the rotation angle, and the intermonomer distance). A detailed analysis was based on the MO topologies and the MTDM and ETDM, the vectors which determine the CD intensities, has been conducted.

We showed that the chiral signal per monomer unit (i.e., the total intensity divided by the number of monomers) increases almost linearly with increasing the oligomer size. The CD signal is also highly sensitive to long-range interunits distances. So, we have obtained useful spectroscopic−structural connections between this intermolecular distance and the exciton bandwidth. The analysis of the transition dipole moment vectors allowed us to accurately assign the magnetic and the electric contributions of the main CD bands, which are essential to explain the relations between the absorption and the CD spectra. The origin of the CD signal, either magnetic or electric, was successfully interpreted from of the topologies of the MOs associated to the one-electronic transitions. Two different MO topologies were described for this type of supramolecular aggregates, named as stacking and antistacking. Thus, from a simple analysis of the MOs connected in each CD band, its magnetic or electric character can be anticipated. Our calculations also showed that small rotation angles provide intense Cotton effects and strong CD bands. As a final remark, we rationale the influence of the various structural factors of supramolecular self-assemblies in connection with the nature of their CD spectroscopic signal, which provides new avenues for structure−spectroscopic relationships.

■ ASSOCIATED CONTENT

Supporting Information. Details of stabilization energies of the oligomers, complete assignment of the more relevant excitation energies for the trimer, electric and magnetic transition dipole vectors, CD spectra using different ab initio basis sets, and topologies of the more relevant molecular orbitals. This material is available free of charge via the Internet at http://pubs.acs.org.

■ AUTHOR INFORMATION

Corresponding Author
*E-mail: ramirez@uma.es.

■ ACKNOWLEDGMENT

Financial support is indebted to DGES-MEC and Junta de Andalucía through research projects CTQ2009-10098-BQU and P09-FQM-4708. B.N.O. thanks the Ministerio de Educación (Spain) for the personal grant FPU-AP2009-2797.

■ REFERENCES

(1) Seeber, G.; Tiedemann, B. E. F.; Raymond, K. N. In *Topics in Current Chemistry*; Crego-Calama, M., Reinhoudt, D. N., Eds.; Springer: Berlin, Germany, 2006; Vol. 265, Chpt. 4.
(2) Soai, K.; Kawasaki, T. In *Topics in Current Chemistry*; Soai, K., Ed.; Springer: Berlin, Germany, 2008; Vol. 284, Chpt. 1.
(3) Raval, R. *Chem. Soc. Rev.* **2009**, *38*, 707–721.
(4) Crassous, J. *Chem. Soc. Rev.* **2009**, *38*, 830–845.
(5) Hoeben, F. J. M.; Jonkheijm, P.; Meijer, E. W.; Schenning, A. P. H. *J. Chem. Rev.* **2005**, *105*, 1491–1546.
(6) Pisula, W.; Tomovic, Z.; Watson, M. D.; Müllen, K.; Kussmann, J.; Ochsenfeld, C.; Metzroth, T.; Gauss, J. *J. Phys. Chem. B* **2007**, *111*, 7481–7487.
(7) (a) J.-M. Lehn. *Supramolecular Chemistry: Concepts and Perspectives*, Wiley-VCH: Weinheim, Germany, 1995. (b) Lehn, J.-M. *Science* **2002**, *295*, 2400–2403.
(8) Meijer, E. W.; Schenning, Albert P. H. J. *Nature* **2002**, *419*, 353–354.
(9) Coquerel, G.; Amabilino, D. B. In *Chirality at the Nanoscale: Nanoparticles, Surfaces, Materials and more*; D. B. Amabilino, D. B., Ed.; Wiley-VCH Verlag: Weinheim, Germany, 2009.
(10) Snatzke, G. In *Circular Dichroism. Principles and Applications*; Berova, N.; Nakanish, K.; Woody, R. W., Eds; Wiley-VCH: New York, 2000; Chpt. 1.
(11) Gawronski, J., Skowronek, P. In *Chiral Analysis*; Busch, K. W.; Busch, M. A., Eds. Elsevier B.V: Amsterdam, The Netherlands, 2006; Chpt. 13.
(12) Nordén, B.; Rodger, A.; Dafford, T. *Linear Dichroism and Circular Dichroism*; RSC Publishing; Cambridge, U.K., 2010; Chpt. 10.
(13) Kuroda, R.; Honma, T. *Chirality* **2000**, *12*, 269–277.
(14) Johannessena, C.; Thulstrup, P. W. *Dalton Trans.* **2007**, 1028–1033.
(15) Castiglioni, E.; Biscarini, P.; Abbate, S. *Chirality* **2009**, *21*, E28–E36.
(16) *Circular Dichroism and the Conformational Analysis of Biomolecules*; Fasman, G. D., Ed.; Plenum Press: New York, 1996.
(17) Lightner, D. A.; Gurst, J. E. *Organic Conformational Analysis and Stereochemistry from Circular Dichroism Spectroscopy*; Wiley-VCH: New York, 2000.
(18) Nordén, B.; Rodger, A.; Dafforn, T. *Linear Dichroism and Circular Dichroism*; RSC Publishing: Cambridge, U.K., 2010; Chpt. 8.
(19) Gottarelli, G.; Lena, S.; Masiero, S.; Pieraccini, S.; Spada, G. P. *Chirality* **2008**, *20*, 471–485.
(20) Lee, C. C.; Grenier, C.; Meijer, E. W.; Schenning, A. P. H. J. *Chem. Soc. Rev.* **2009**, *38*, 671–683.
(21) Nieto-Ortega, B.; Ramirez, F. J.; Hennrich, G.; Gomez-Lor, B.; Casado, J.; Lopez Navarrete, J. T. *J. Phys. Chem. B* **2010**, *114*, 5710–5717.

(22) Smulders, M. M. J.; Stals, P. J. M.; Mes, T.; Paffen, T. F. E.; Schenning, A. P. H. J.; Palmans, A. R. A.; Meijer, E. W. *J. Am. Chem. Soc.* **2010**, *132*, 621–626.
(23) van Gorp, J. J.; Vekemans, J. A. J. M.; Meijer, E. W. *J. Am. Chem. Soc.* **2002**, *124*, 14759–14769.
(24) Steed, J. W.; Atwood, J. L. *Supramolecular Chemistry*, Wiley: New York, 2009, Chpt. 10.
(25) Frisch, M. J.; Trucks, G. W.; Schlegel, H. B.; Scuseria, G. E.; Robb, M. A.; Cheeseman, J. R.; Scalmani, G.; Barone, V.; Mennucci, B.; Petersson, G. A.; Nakatsuji, H.; Caricato, M.; Li, X.; Hratchian, H. P.; Izmaylov, A. F.; Bloino, J.; Zheng, G.; Sonnenberg, J. L.; Hada, M.; Ehara, M.; Toyota, K.; Fukuda, R.; Hasegawa, J.; Ishida, M.; Nakajima, T.; Honda, Y.; Kitao, O.; Nakai, H.; Vreven, T.; Montgomery, J. A., Jr.; Peralta, J. E.; Ogliaro, F.; Bearpark, M.; Heyd, J. J.; Brothers, E.; Kudin, K. N.; Staroverov, V. N.; Kobayashi, R.; Normand, J.; Raghavachari, K.; Rendell, A.; Burant, J. C.; Iyengar, S. S.; Tomasi, J.; Cossi, M.; Rega, N.; Millam, N. J.; Klene, M.; Knox, J. E.; Cross, J. B.; Bakken, V.; Adamo, C.; Jaramillo, J.; Gomperts, R.; Stratmann, R. E.; Yazyev, O.; Austin, A. J.; Cammi, R.; Pomelli, C.; Ochterski, J. W.; Martin, R. L.; Morokuma, K.; Zakrzewski, V. G.; Voth, G. A.; Salvador, P.; Dannenberg, J. J.; Dapprich, S.; Daniels, A. D.; Farkas, Ö.; Foresman, J. B.; Ortiz, J. V.; Cioslowski, J.; Fox, D. J. *Gaussian 09*, revision A.2; Gaussian, Inc.: Wallingford, CT, 2009.
(26) Becke, A. D. *J. Chem. Phys.* **1993**, *98*, 5648–5652.
(27) Stephens, P. J.; Devlin, F. J.; Chabalowski, C. F.; Frisch, M. J. *J. Phys. Chem.* **1994**, *98*, 11623–11627.
(28) Kim, K.; Jordan, K. D. *J. Phys. Chem.* **1994**, *98*, 10089–10094.
(29) Yanai, T.; Tew, D. P.; Nicholas, N. C. *Chem. Phys. Lett.* **2004**, *393*, 51–57.
(30) Peach, M. J. G.; Tellgren, E. I.; Salek, P.; Helgaker, T.; Tozer, D. J. *J. Phys. Chem. A* **2007**, *111*, 11930–11935.
(31) Limacher, P. A.; Mikkelsen, K. V.; L_thi, H. P. *J. Chem. Phys.* **2009**, *130*, 194114/1–194114/7.
(32) Jacquemin, D.; Wathelet, V.; Perpete, E. A.; Adamo, C. *J. Chem. Theory Comput.* **2009**, *5*, 2420–2435.
(33) Zhang, J.; Guo, X.; Cao, Z. *J. Chem. Phys.* **2009**, *131*, 144307/1–144307/7.
(34) Borini, S.; Limacher, P. A.; Lüthi, H. P. *J. Phys. Chem. A* **2010**, *114*, 2221–2229.
(35) Rivera- Rivera-Fuentes, P.; Alonso-Gómez, J. L.; Petrovic, A. G.; Seiler, P.; Santoro, F.; Harada, N.; Berova, N.; Rzepa, H. S.; Diederich, F. *Chem. Eur. J. A* **2010**, *16*, 9796–9807.
(36) Hariharan, P. C.; Pople, J. A. *Theor. Chim. Acta* **1973**, *28*, 213–222.
(37) Clark, T.; Chandrasekhar, J.; Spitznagel, G. W.; Schleyer, P. V. R. *J. Comput. Chem.* **1983**, *4*, 294–301.
(38) Runge, E.; Gross, E. K. U. *Phys. Rev. Lett.* **1984**, *52*, 997–1000.
(39) Gross, E. K. U.; Kohn, W. *Adv. Quantum Chem.* **1990**, *21*, 255–294.
(40) Matile, S.; Berova, N.; Nakanishi, K.; Fleischhauer, J.; Woody, R. W. *J. Am. Chem. Soc.* **1996**, *118*, 5198–5206.
(41) Lewis, F. D.; Liu, X. Y.; Wu., Y. S.; Zuo, X. B. *J. Am. Chem. Soc.* **2003**, *125*, 12729–12731.
(42) Tsubaki, K.; Takaishi, K.; Tanaka, H.; Miura, M.; Kawabata, T. *Org. Lett.* **2006**, *8*, 2587–2590.
(43) Van Dijk, L.; Bobbert, P. A.; Spano, F. C. *J. Phys. Chem. B* **2010**, *114*, 817–825.